




## Moving smectic phase and transverse mode locking in driven vortex matter

S. Maegochi <sup>\*</sup>, K. Ienaga , and S. Okuma <sup>†</sup>

*Department of Physics, Tokyo Institute of Technology, 2-12-1 Ohokayama, Meguro-ku, Tokyo 152-8551, Japan*



(Received 14 March 2022; revised 3 June 2022; accepted 27 June 2022; published 29 July 2022)

Out-of-equilibrium systems exhibit various dynamic phases with different degrees of order. A moving smectic phase with transverse periodicity is one of the ordered states, which is theoretically expected to be generic to driven two-dimensional systems. However, a comprehensive dynamic phase diagram, including the moving smectic phase, has not been obtained because of lack of suitable experimental methods. Here we study dynamic phases of driven vortex matter in an amorphous  $\text{Mo}_x\text{Ge}_{1-x}$  film by using two-step measurements of transient voltage in response to mutually perpendicular driving currents. We find dynamic orderings from the plastic flow to the anisotropic smectic flow and from the anisotropic smectic flow to the isotropic moving Bragg glass as a function of the current. Convincing evidence of the moving smectic phase is obtained from the first transverse mode locking (ML) with signals larger than those of longitudinal ML, indicating the higher transverse order than the longitudinal one. Transverse ML developed here is useful to detect the anisotropic periodicity in driven media.

DOI: [10.1103/PhysRevResearch.4.033085](https://doi.org/10.1103/PhysRevResearch.4.033085)

### I. INTRODUCTION

Condensed-matter systems often exhibit a variety of ordering phenomena away from equilibrium [1–3]. A general question is how the disordered system recovers its order dynamically. Dynamical ordering of a vortex system interacting with a random substrate [4–23] is a prominent example where an applied current  $I$  (driving force) reduces the coupling between vortices and random pinning centers, giving rise to various dynamic phases with different degrees of order. With an increase in  $I$ , an initial pinned system undergoes a depinning transition at a depinning current  $I_d$  [3,24–29]. Just above  $I_d$ , the system is in a disordered plastic flow state dominated by pinning. At sufficiently large  $I$ , the pinning becomes ineffective and the disordered flow finally reorders into an isotropic moving Bragg glass, where the vortices form a sixfold structure. Between the plastic flow and the moving Bragg glass state, a different type of ordered state called a smectic flow has been proposed by several theoretical works and simulations [7–12]. The smectic flow is characterized by anisotropic structures with long-range order in the direction transverse to the drive and is likely to be generic to driven two-dimensional (2D) systems [3,7] such as Wigner crystals [30], charge transport in metallic dots [31], skyrmions [32], and emulsions [33]. Despite its ubiquitousness, clear evidence of the moving smectic phase has not yet been obtained as a

function of driving  $I$ . The smectic structure of vortex flow was observed by a magnetic decoration experiment [34,35], in which vortices were driven by a field gradient. The available field  $B$  and average vortex velocity  $v$  were limited to below several tens of millitesla and  $\approx 1 \mu\text{m/s}$  (i.e., a slowly creeping regime), respectively, and the driving force was not changed systematically. Thus the dynamical ordering from the plastic flow to smectic flow and that into the moving Bragg glass state have not been revealed by any experiment.

In this work, we observe the successive dynamic orderings through these distinct dynamic phases as a function of  $I$  and provide clear evidence of the moving smectic phase in the large velocity regime ( $\approx 1 \text{ m/s}$ ). In order to construct the dynamic phase diagram, we use a two-step protocol consisting of mutually perpendicular drives [36]. This protocol is a modification of two-step measurements using successive parallel drives [37,38], which allow us to detect the degree of order of vortex configurations. Here in the first-step measurement, we drive the vortices in one ( $y$ ) direction for a long time and freeze the vortex configuration in the steady state by shutting off the current abruptly. In the second-step measurement, we apply the driving force of the same magnitude in the ( $x$ ) direction perpendicular to the first drive and measure the time-dependent voltage  $V(t)$ . We find that the vortices immediately after applying the second drive move more easily for low drives, less easily for intermediate drives, and almost equally for sufficiently high drives. The results indicate the dynamic ordering from the plastic flow to the anisotropic smectic flow and that from the anisotropic smectic flow to the isotropic moving Bragg glass induced by  $I$ .

Also, we obtain more convincing evidence of the moving smectic phase by means of mode-locking (ML) measurements [39–58]. ML is a useful method to detect the periodicity in driven media such as charge-density waves [39–42], Josephson junction arrays [43,44], colloids on ordered substrates

\*maegochi.s.aa@m.titech.ac.jp

†sokuma@o.cc.titech.ac.jp

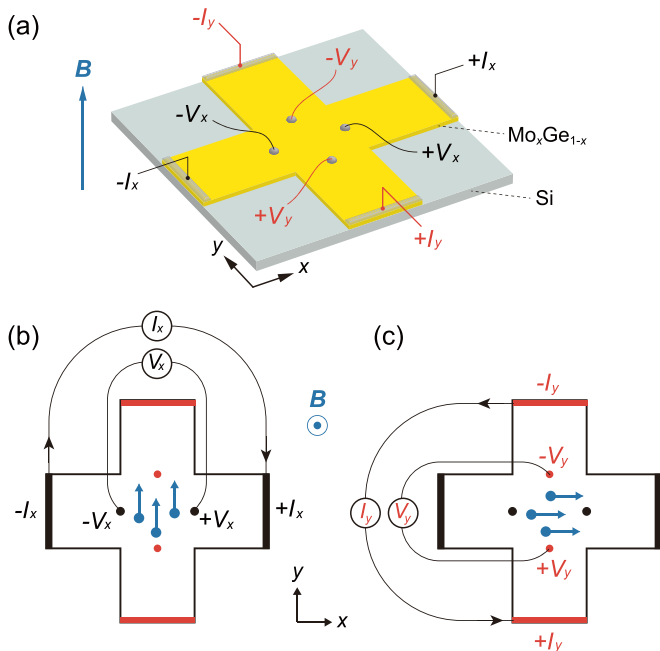


FIG. 1. (a) Schematics of the cross-shaped film of amorphous  $\text{Mo}_x\text{Ge}_{1-x}$  on the Si substrate and the arrangement of electrodes. The magnetic field  $B$  is applied perpendicular to the film surface. (b) Experimental setup for the first-step measurements and the second-step measurements of parallel drive (Drive  $y$ ). (c) Experimental setup for the second-step measurements of perpendicular drive (Drive  $x$ ). Blue dots and arrows illustrate the vortex motion due to the Lorentz-like force.

[45], and superconducting vortices [46–58]. In the conventional ML experiments, an interference signal analogous to Shapiro steps [59] is observed in dc  $I - V$  characteristics by superimposing longitudinal rf currents. In this work, in addition to the longitudinal ML, we conduct transverse ML measurements, in which the rf current transverse to the dc current  $I$  is superimposed and first observe transverse ML signals [60]. The interference signals of transverse ML are considerably larger than those of longitudinal ML, supporting a picture of the moving smectic phase that the transverse order is higher than the longitudinal order.

## II. EXPERIMENTAL SETUP

The sample was a 280-nm-thick cross-shaped film of amorphous  $\text{Mo}_x\text{Ge}_{1-x}$  ( $x \approx 0.78$ ) with weak random pinning, which was prepared by rf sputtering deposition onto a Si substrate held at room temperature. A shape of the sample with an arrangement of current ( $\pm I_x, \pm I_y$ ) and voltage ( $\pm V_x, \pm V_y$ ) electrodes is schematically shown in Fig. 1(a), where the size of the intersection is about  $2 \times 2 \text{ mm}^2$ . We conducted four probe measurements in the  $x$  and  $y$  directions using the ( $\pm I_x, \pm V_x$ ) and ( $\pm I_y, \pm V_y$ ) electrodes, respectively, and obtained an identical critical temperature  $T_c = 6.2 \text{ K}$  independent of the directions, indicating the uniformity of the film. The field  $B$  was applied perpendicular to the film surface. All of the data were taken at 3.6 K and 1.0 T, corresponding to the Bragg glass phase at equilibrium [29,61]. The size of the vortex core and the range of repulsive vortex-vortex inter-

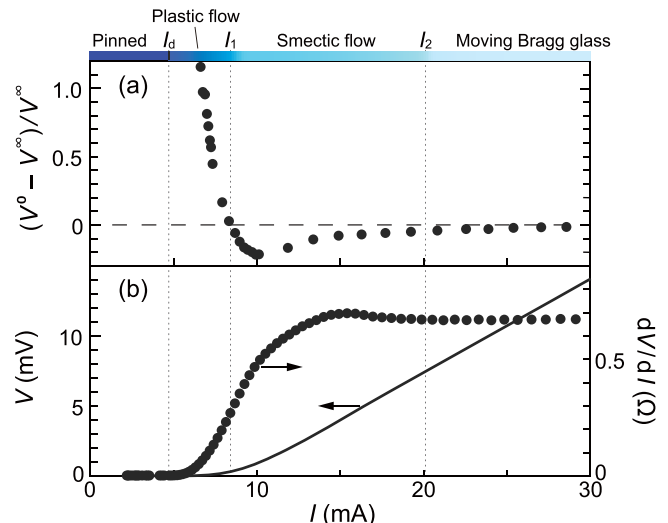


FIG. 2. (a)  $I$  dependence of  $(V^0 - V^\infty)/V^\infty$  extracted from  $V(t)$  in response to the perpendicular second drive (Drive  $x$ ), where  $V^0$  and  $V^\infty$  are initial and steady-state voltages, respectively. A horizontal dashed line represents the location of zero. The dynamic phase diagram is shown above (a). (b)  $I - V$  characteristics (solid line) and  $dV/dI$  (circles). Vertical dotted lines mark the location of  $I_d$ ,  $I_1$  at which a sign reversal of  $(V^0 - V^\infty)/V^\infty$  occurs, and  $I_2$  at which  $dV/dI$  flattens out.

action characterized by the superconducting coherence length and London penetration depth are estimated to be  $\approx 1 \times 10$  and  $\approx 10^2 \text{ nm}$ , respectively [62]. The sample was immersed in liquid  $^4\text{He}$  to reduce possible heating. The average velocity  $v$  of vortices was estimated from the voltage induced by vortex motion,  $V = vBl$ , where  $l (= 1.95 \text{ mm})$  is the distance between voltage contacts. In the two-step measurements, the transient voltage  $V(t)$  in response to a square current with a sharp rise time of  $0.5 \mu\text{s}$  was measured using an oscilloscope (Rohde and Schwarz RTO2024) with resolution of 10 MHz [63,64] and the steady-state voltage was denoted as  $V^\infty [\equiv V(t \rightarrow \infty)]$ . Figure 2(b) shows the  $I - V$  characteristics, where the depinning current  $I_d = 4.7 \text{ mA}$  is defined by a  $10^{-8} \text{ V}$  criterion. Upward curvature just above  $I_d$  indicates the plastic depinning. Compared with the conventional strip-shaped film, some current may leak in wider central zone in our cross-shaped film. This may lead to an overestimation of the absolute value of  $I$  but does not influence the discussion which follows.

## III. RESULTS AND DISCUSSION

### A. Two-step measurements

In the first-step measurements, as shown in Fig. 1(b), we drive the vortices in the  $y$  direction by applying the Lorentz-like driving force (current  $I$ ) in the  $y$  direction (minus  $x$  direction), yielding  $V^\infty = 0.01 \text{ mV}$ , corresponding to the plastic flow regime, and shut off the driving force ( $I$ ) to freeze the vortex configuration in the steady state. Then, in the second-step measurements, we apply a driving force of the same magnitude in the same direction as the first one (i.e., in the  $y$  direction), which we call a parallel second drive, Drive

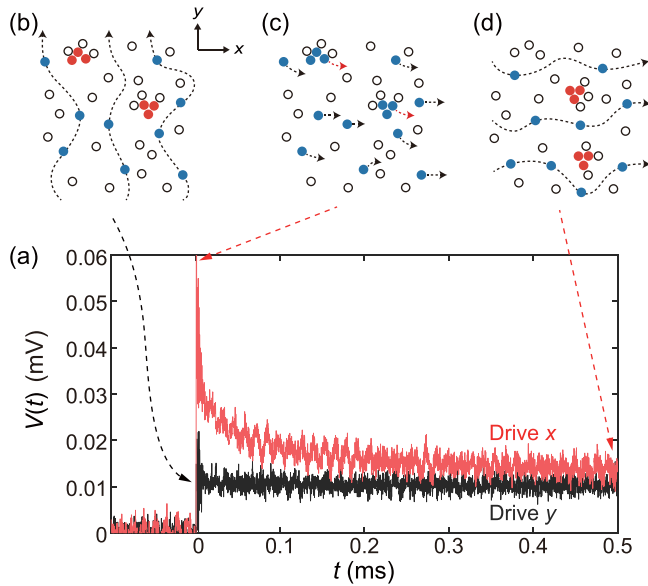


FIG. 3. Directional fragility of the clogging. (a) Voltage responses  $V(t)$  to the second drive parallel (black) and perpendicular (red) to the first drive applied in the  $y$  direction. (b–d) Schematics of vortex flow at the beginning of the parallel second drive (Drive  $y$ ) (b) and at the beginning (c) and at the end (d) of the perpendicular second drive (Drive  $x$ ). Open circles represent the pinned vortices. Blue and red dots illustrate the flowing and trapped vortices, respectively.

$y$ . We also conduct the second-step measurements applying a driving force rotated by  $90^\circ$  clockwise relative to the first one as shown in Fig. 1(c), which we call a perpendicular second drive, Drive  $x$ . In Fig. 3(a), voltage responses  $V(t)$  to Drives  $y$  and  $x$  are shown by black and red lines, respectively. For Drive  $y$ , the voltage induced by vortex motion rises steeply, reaching immediately a steady-state value  $V^\infty$  and no relaxation is observed. In contrast, for Drive  $x$ , the voltage exhibits a large initial rise exceeding  $V^\infty$  and a subsequent decrease toward  $V^\infty$ . The results indicate that after applying Drive  $x$ , the vortices are temporarily more mobile than in the steady-state flow state of the first-step measurements, while the application of Drive  $y$  does not change the flow state.

The observed anisotropic responses to the second drives are explained in terms of directional fragility of the clogging phenomena [36,65–68]. Let us consider the flow of particles that is hindered or blocked in the presence of walls and constrictions. Such a flow is easily recovered by changing the direction of the driving force. The two-step measurements shown in Fig. 3(a) were performed in the low velocity regime just above  $I_d$ , where the steady-state flow is the disordered plastic flow, containing many pinned vortices. Since the pinning centers in our film [28] are randomly distributed, the pinned vortices are mostly isolated, while some can form wall-like structures [65–68]. At the end of the first-step measurement, some portion of flowing vortices is trapped by the walls, as schematically illustrated by red dots in Fig. 3(b). When we apply the parallel second drive (Drive  $y$ ), these vortices remain still trapped on the walls and no change in  $V(t)$  is expected. By contrast, when the perpendicular second drive

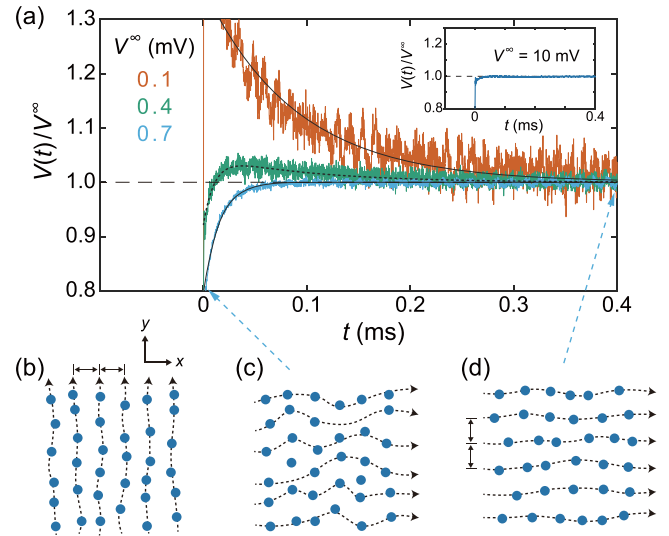


FIG. 4. Directional robustness of the smectic flow. (a) Voltage responses  $V(t)/V^\infty$  to the perpendicular second drive (Drive  $x$ ) yielding  $V^\infty = 0.1, 0.4,$  and  $0.7$  mV from top to bottom. Solid and dotted lines represent fits to the data (see text), and a horizontal dashed line marks the steady-state value of unity. Inset:  $V(t)/V^\infty$  subjected to Drive  $x$  with  $V^\infty = 10$  mV. (b) The vortex configuration at the end of the first drive in the smectic flow regime. Dotted lines represent flow channels with periodicity in the  $x$  direction. (c) Vortex flow just after applying Drive  $x$  to the frozen configuration in (b), and (d) that subjected to long-time Drive  $x$ , forming smectic flow with periodicity in the  $y$  direction.

(Drive  $x$ ) is applied, some vortices trapped on the walls can escape and take part in the flow, as schematically illustrated by red arrows in Fig. 3(c), which gives rise to a large rise of  $V(t)$  at  $t \approx 0$ . However, the flowing vortices are gradually captured by other walls again, as schematically shown by red dots in Fig. 3(d), and  $V(t)$  decreases monotonically toward  $V^\infty$ , as seen by the red line in Fig. 3(a).

We also perform the same two-step measurements using larger driving forces ( $V^\infty$ ). Figure 4(a) shows the voltage responses to the perpendicular second drives (Drive  $x$ ), where  $V(t)$  is normalized by the steady-state voltage of  $V^\infty = 0.1, 0.4,$  and  $0.7$  mV from top to bottom. For  $V^\infty = 0.1$  mV,  $V(t)$  still shows a monotonic decrease similar to that seen in Fig. 3(a). For  $V^\infty = 0.4$  mV, however, a decreasing relaxation is significantly suppressed, and for  $V^\infty = 0.7$  mV, an initial rise at  $t \approx 0$  exceeding  $V^\infty$  is no longer visible and  $V(t)$  exhibits a monotonic increasing behavior.

The decreasing relaxation observed for  $V^\infty = 0.1$  mV indicates that the plastic flow with clogging still survives. With an increase in  $V^\infty$ , the number of pinned vortices that form walls decreases and the clogging mechanism is suppressed, and for  $V^\infty = 0.7$  mV, the clogging mechanism is subject to or replaced by an alternative mechanism. Since the increasing relaxation in  $V(t)$  appears only in the relatively high velocity regime ( $I > 8.4$  mA), we attribute it to the directional robustness of the smectic flow, as schematically illustrated in Figs. 4(b)–4(d): At the end of the first-step measurements, the vortices form straight 1D flow channels in the  $y$  direction, as shown in Fig. 4(b). Due to the smectic nature, these channels

have the transverse periodicity but the vortices in channels possess no longitudinal order. When the perpendicular second drive (Drive  $x$ ) is applied, these vortices cannot immediately form straight flow channels in the  $x$  direction; instead, they form winding channels, as shown in Fig. 4(c), with lower mobility. After undergoing rearrangements of the flow channels, the flowing vortices finally reorganize into the 1D smectic channels, as shown in Fig. 4(d), thus accounting for the monotonic increase in  $V(t)$  and relaxation toward  $V^\infty$ . The monotonic relaxation curve for  $V^\infty = 0.1$  mV, which is due to the directional fragility of the clogging, and that for  $V^\infty = 0.7$  mV, which is due to the directional robustness of the smectic flow, are well fitted using a single exponential function, as shown by black solid lines in Fig. 4(a). Meanwhile,  $V(t)$  for  $V^\infty = 0.4$  mV exhibits a nonmonotonic relaxation, which is fitted to the sum of the two exponential terms, as shown with a dotted line, indicative of the coexistence of the clogging and smectic mechanisms. We also find that the relaxation of  $V(t)$  almost disappears at sufficiently high drive,  $V^\infty = 10$  mV, as shown in the inset to Fig. 4(a). This implies the reduced anisotropy inherent to smectic flow and emergence of the isotropic moving Bragg glass state.

In Fig. 2(a), we plot  $(V^0 - V^\infty)/V^\infty$  extracted from  $V(t)$  in response to Drive  $x$  with various amplitudes against  $I$ , where  $V^0[\equiv V(t = 2 \mu\text{s})]$  is the initial voltage at  $t = 2 \mu\text{s}$ , corresponding to the response time of the amplifier. A sign reversal from positive to negative occurs at 8.4 mA ( $\equiv I_1$ ), indicating that the flow state crosses over from the plastic flow with clogging to the smectic flow around  $I_1$ . After showing a minimum,  $(V^0 - V^\infty)/V^\infty$  increases gradually and converges to zero at sufficiently high  $I \approx 20$  mA. This value is very close to 20 mA ( $\equiv I_2$ ) at which the differential resistance  $dV/dI$  in Fig. 2(b) flattens out.  $I_2$  is usually considered as an onset of the moving Bragg glass state [4,10,15,22]. Thus we display the dynamic phase diagram of vortices revealed from the two-step measurements above Fig. 2(a), which shows that the vortex flow state crosses over from the plastic flow to smectic flow around  $I_1$  and from the smectic flow to moving Bragg glass around  $I_2$ .

### B. Transverse and longitudinal ML

To demonstrate the smectic order of vortices in motion more directly, we carried out the ML experiments [39–58]. ML is a dynamic interference between the internal frequency  $f_{\text{int}}$  of the periodic media driven over pinning potentials and the external frequency  $f_{\text{ext}}$  of the rf drive superimposed on the dc drive. When the two frequencies satisfy the relation  $pf_{\text{int}} = qf_{\text{ext}}$  with integers  $(p, q)$ , ML steps in the  $I - V$  curves or peak structures of the differential conductance  $dI/dV$  appear at  $V_{p/q} = (p/q)f_{\text{ext}}aBl$ , where  $a$  is the period of vortex lattices in the dc flow direction. Since the vortex lattice can orient with its principal axis parallel and perpendicular to the flow direction, two values of  $a$  are possible [47,55,56,69]:  $a = a_0$  and  $a = \sqrt{3}a_0$  for parallel and perpendicular orientations, respectively, where  $a_0 = (2\Phi_0/\sqrt{3}B)^{1/2}$  is a lattice spacing ( $\approx 50$  nm at 1.0 T).

Figure 5(a) displays  $dI/dV$  of conventional longitudinal ML, where the 25-MHz rf current  $I_{\text{rf}}$  in the  $x$  direction with different amplitudes 9.18, 9.86, and 10.54 mA from bottom to

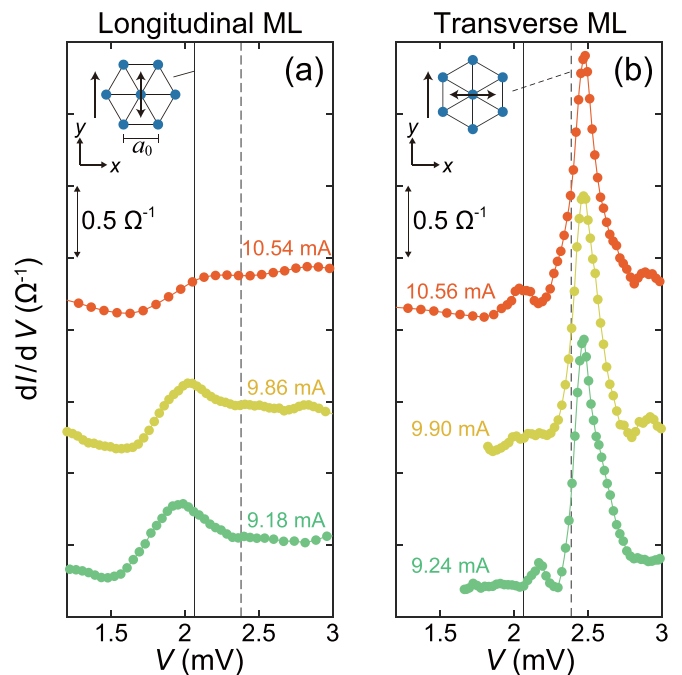


FIG. 5.  $dI/dV$  versus  $V$  for longitudinal ML (a) and transverse ML (b). The amplitudes  $I_{\text{rf}}$  of superimposed 25-MHz rf current are shown in each figure. Curves are vertically shifted for clarity. Vertical solid and dashed lines indicate the calculated values of ML peaks for the perpendicular and parallel orientations, respectively. The inset illustrates schematics of vortex lattices moving with perpendicular (a) and parallel (b) orientations. The flow directions by dc and ac drives are shown by single and double arrows, respectively.  $a_0$  is the lattice spacing.

top is superimposed on the dc current  $I$  in the same  $x$  direction, and hence both the dc and ac driving forces are exerted in the  $y$  direction. In the present experiment,  $f_{\text{ext}} \approx 25$  MHz is the maximum frequency available for the ML measurement. The ML peaks are observed at  $V \approx 2$  mV, corresponding to the smectic flow state. This value is close to  $V_{1/2}$  with  $a = \sqrt{3}a_0$ , as marked by a vertical solid line, indicating the perpendicular orientation, as schematically illustrated in the inset. Figure 5(b) shows  $dI/dV$  of transverse ML, where the 25-MHz  $I_{\text{rf}}$  with different amplitude 9.24, 9.90, and 10.56 mA from bottom to top is superimposed in the  $y$  direction perpendicular to the dc current. To our knowledge, this is the first experimental observation of transverse ML. Unlike longitudinal ML, the fundamental ML peaks are observed at  $V \approx 2.5$  mV, which again corresponds to the smectic flow state but is close to  $V_{1/1}$  with  $a = a_0$ , as marked by a vertical dashed line. This indicates the parallel orientation, as schematically shown in the inset.

In our previous work, we have found the velocity-induced reorientation of a vortex lattice from a perpendicular to a parallel orientation, which occurs when a characteristic time  $\tau$  for the vortex to travel  $a_0$  decreases down to  $\tau_{\text{th}} \approx 10$  ns, with an increase in the effective (total) velocity [56]. In this work, the result on longitudinal ML certainly satisfies the condition  $\tau (\approx 25 \text{ ns}) > \tau_{\text{th}}$ , consistent with the observation of the perpendicular orientation. For transverse ML where the parallel orientation is observed, however, the net velocity in

the dc flow direction does not exceed that for longitudinal ML, because dc and ac components are orthogonal. Therefore the lattice rotation from the perpendicular to parallel orientation is not explained by the increased velocity. From the inset to Figs. 5(a) and 5(b), we note that both lattices take a perpendicular orientation with respect to the direction of the ac drive. It has been predicted numerically that the vortex lattice tends to order with its principal lattice vector aligned perpendicular to the direction of oscillating motion [69], consistent with the present results.

The most striking feature seen from Fig. 5 is that the peak intensity of transverse ML is considerably higher than that of longitudinal ML. This means that at ML, more vortices move coherently by the transverse ac drive than the longitudinal one. This result is well explained by the smectic flow picture. It has been shown by several simulations [9,10,12] that the smectic flow under the dc drive involves some aligned dislocations with their Burgers vector in the direction of the driving force. Once the dislocations glide, adjacent smectic flow channels easily slip past each other. When the longitudinal ac drive is superimposed, the phase of vortex motion between coupled channels is locked. However, the occurrence of the phase slip between the channels prevents the entire system from being phase locked, which explains the relatively small peaks of longitudinal ML. In contrast, when the transverse ac drive is superimposed, all channels are forced to move transversely in the same phase because of the presence of the transverse periodicity in the smectic flow [7–12]. This gives rise to the large peaks of transverse ML, as seen in Fig. 5(b). Similar geometrical constraint effects are observed in other elastic media such as charge-density wave systems, where inherent longitudinal periodicity results in a sharp longitudinal ML

resonance [39–42]. We have shown in this work that both the transverse and the longitudinal ML resonances are useful to detect the anisotropic periodicity in driven media, in the present case, the dynamically induced transverse periodicity of smectic flow of fast driven vortices with  $v \approx 1$  m/s, where a visualization technique is not available.

#### IV. CONCLUSION

We studied the dynamic phases of driven vortices in response to mutually perpendicular drives ( $I$ ) and find the dynamic orderings from the plastic flow to the anisotropic smectic flow and from the anisotropic smectic flow to the isotropic moving Bragg glass induced by  $I$ . The directional fragility associated with clogging is observed in the plastic flow. Convincing evidence of the moving smectic phase intervening between the plastic flow and the moving Bragg glass phase is obtained from the first transverse ML with resonance signals larger than those of longitudinal ML, indicating the higher transverse order than the longitudinal one. We show that transverse ML developed here is a useful method to detect the anisotropic periodicity in driven media.

#### ACKNOWLEDGMENTS

We thank S. Kaneko for fruitful discussions. This work was supported by a Grant-in-Aid for Scientific Research on Innovative Areas (KAKENHI Grant No. 20H05266), Challenging Research (KAKENHI Grant No. 21K18598), Young Scientists (KAKENHI Grant No. 20K14413), and JSPS Fellows (KAKENHI Grant No. 20J21425) from the Japan Society for the Promotion of Science.

- 
- [1] G. M. Whitesides and B. Grzybowski, Self-assembly at all scales, *Science* **295**, 2418 (2002).
  - [2] T. Vicsek and A. Zafeiris, Collective motion, *Phys. Rep.* **517**, 71 (2012).
  - [3] C. Reichhardt and C. J. Olson Reichhardt, Depinning and nonequilibrium dynamic phases of particle assemblies driven over random and ordered substrates: A review, *Rep. Prog. Phys.* **80**, 026501 (2017).
  - [4] A.-C. Shi and A. J. Berlinsky, Pinning and  $I$ - $V$  Characteristics of a Two-Dimensional Defective Flux-Line Lattice, *Phys. Rev. Lett.* **67**, 1926 (1991).
  - [5] A. E. Koshelev and V. M. Vinokur, Dynamic Melting of the Vortex Lattice, *Phys. Rev. Lett.* **73**, 3580 (1994).
  - [6] T. Giamarchi and P. Le Doussal, Moving Glass Phase of Driven Lattices, *Phys. Rev. Lett.* **76**, 3408 (1996).
  - [7] L. Balents, M. C. Marchetti, and L. Radzihovsky, Nonequilibrium steady states of driven periodic media, *Phys. Rev. B* **57**, 7705 (1998).
  - [8] P. Le Doussal and T. Giamarchi, Moving glass theory of driven lattices with disorder, *Phys. Rev. B* **57**, 11356 (1998).
  - [9] K. Moon, R. T. Scalettar, and G. T. Zimányi, Dynamical Phases of Driven Vortex Systems, *Phys. Rev. Lett.* **77**, 2778 (1996).
  - [10] C. J. Olson, C. Reichhardt, and F. Nori, Nonequilibrium Dynamic Phase Diagram for Vortex Lattices, *Phys. Rev. Lett.* **81**, 3757 (1998).
  - [11] A. B. Kolton, D. Domínguez, and N. Grønbech-Jensen, Hall Noise and Transverse Freezing in Driven Vortex Lattices, *Phys. Rev. Lett.* **83**, 3061 (1999).
  - [12] H. Fangohr, D. J. Cox, and P. A. J. de Groot, Vortex dynamics in two-dimensional systems at high driving forces, *Phys. Rev. B* **64**, 064505 (2001).
  - [13] S. Ryu, M. HELLERQVIST, S. Doniach, A. Kapitulnik, and D. Stroud, Dynamical Phase Transition in a Driven Disordered Vortex Lattice, *Phys. Rev. Lett.* **77**, 5114 (1996).
  - [14] M.-C. Miguel and S. Zapperi, Tearing transition and plastic flow in superconducting thin films, *Nat. Mater.* **2**, 477 (2003).
  - [15] S. Bhattacharya and M. J. Higgins, Dynamics of a Disordered Flux Line Lattice, *Phys. Rev. Lett.* **70**, 2617 (1993).
  - [16] U. Yaron, P. L. Gammel, D. A. Huse, R. N. Kleiman, C. S. Oglesby, E. Bucher, B. Batlogg, D. J. Bishop, K. Mortensen, and K. N. Clausen, Structural evidence for a two-step process in the depinning of the superconducting flux-line lattice, *Nature (London)* **376**, 753 (1995).
  - [17] A. C. Marley, M. J. Higgins, and S. Bhattacharya, Flux Flow Noise and Dynamical Transitions in a Flux Line Lattice, *Phys. Rev. Lett.* **74**, 3029 (1995).
  - [18] M. C. HELLERQVIST, D. Ephron, W. R. White, M. R. Beasley, and A. Kapitulnik, Vortex Dynamics in Two-Dimensional Amorphous  $\text{Mo}_{77}\text{Ge}_{23}$  Films, *Phys. Rev. Lett.* **76**, 4022 (1996).

- [19] F. Pardo, F. De La Cruz, P. L. Gammel, C. S. Oglesby, E. Bucher, B. Batlogg, and D. J. Bishop, Topological Defects in the Flux-Line Lattice and Their Relationship to the Critical Current of a Type-II Superconductor, *Phys. Rev. Lett.* **78**, 4633 (1997).
- [20] A. M. Troyanovski, J. Aarts, and P. H. Kes, Collective and plastic vortex motion in superconductors at high flux densities, *Nature (London)* **399**, 665 (1999).
- [21] Z. L. Xiao, E. Y. Andrei, and M. J. Higgins, Flow Induced Organization and Memory of a Vortex Lattice, *Phys. Rev. Lett.* **83**, 1664 (1999).
- [22] Z. L. Xiao, E. Y. Andrei, P. Shuk, and M. Greenblatt, Equilibration and Dynamic Phase Transitions of a Driven Vortex Lattice, *Phys. Rev. Lett.* **85**, 3265 (2000).
- [23] Y. Togawa, R. Abiru, K. Iwaya, H. Kitano, and A. Maeda, Direct Observation of the Washboard Noise of a Driven Vortex Lattice in a High-Temperature Superconductor,  $\text{Bi}_2\text{Sr}_2\text{CaCu}_2\text{O}_y$ , *Phys. Rev. Lett.* **85**, 3716 (2000).
- [24] D. P. Daroca, G. S. Lozano, G. Pasquini, and V. Bekkeris, Depinning and dynamics of ac driven vortex lattices in random media, *Phys. Rev. B* **81**, 184520 (2010).
- [25] S. Okuma, Y. Tsugawa, and A. Motohashi, Transition from reversible to irreversible flow: Absorbing and depinning transitions in a sheared-vortex system, *Phys. Rev. B* **83**, 012503 (2011).
- [26] S. Okuma and A. Motohashi, Critical behavior associated with transient dynamics near the depinning transition, *New J. Phys.* **14**, 123021 (2012).
- [27] G. Shaw, P. Mandal, S. S. Banerjee, A. Niazi, A. K. Rastogi, A. K. Sood, S. Ramakrishnan, and A. K. Grover, Critical behavior at depinning of driven disordered vortex matter in  $2H\text{-NbS}_2$ , *Phys. Rev. B* **85**, 174517 (2012).
- [28] Y. Kawamura, S. Moriya, K. Ienaga, S. Kaneko, and S. Okuma, Nonequilibrium depinning transition of ac driven vortices with random pinning, *New J. Phys.* **19**, 093001 (2017).
- [29] T. Kaji, S. Maegochi, K. Ienaga, S. Kaneko, and S. Okuma, Critical behavior of nonequilibrium depinning transitions for vortices driven by current and vortex density, *Sci. Rep.* **12**, 1542 (2022).
- [30] C. Reichhardt, C. J. Olson, N. Grønchech-Jensen, and F. Nori, Moving Wigner Glasses and Smectics: Dynamics of Disordered Wigner Crystals, *Phys. Rev. Lett.* **86**, 4354 (2001).
- [31] C. Reichhardt and C. J. Olson Reichhardt, Charge Transport Transitions and Scaling in Disordered Arrays of Metallic Dots, *Phys. Rev. Lett.* **90**, 046802 (2003).
- [32] S. A. Diaz, C. J. O. Reichhardt, D. P. Arovas, A. Saxena, and C. Reichhardt, Fluctuations and noise signatures of driven magnetic skyrmions, *Phys. Rev. B* **96**, 085106 (2017).
- [33] M. Le Blay, M. Adda-Bedia, and D. Bartolo, Emergence of scale-free smectic rivers and critical depinning in emulsions driven through disorder, *Proc. Natl. Acad. Sci. USA* **117**, 13914 (2020).
- [34] F. Pardo, F. de la Cruz, P. L. Gammel, E. Bucher, and D. J. Bishop, Observation of smectic and moving-Bragg-glass phases in flowing vortex lattices, *Nature (London)* **396**, 348 (1998).
- [35] M. Marchevsky, J. Aarts, and P. H. Kes, Depinning and anisotropic order in flowing and static vortex lattices in  $\text{NbSe}_2$  studied with magnetic decoration, *Phys. Rev. B* **60**, 14601 (1999).
- [36] C. Reichhardt and C. J. O. Reichhardt, Jamming, fragility and pinning phenomena in superconducting vortex systems, *Sci. Rep.* **10**, 11625 (2020).
- [37] M. Dobroka, Y. Kawamura, K. Ienaga, S. Kaneko, and S. Okuma, Memory formation and evolution of the vortex configuration associated with random organization, *New J. Phys.* **19**, 053023 (2017).
- [38] S. Maegochi, M. Dobroka, K. Ienaga, S. Kaneko, and S. Okuma, Time evolution of the vortex configuration associated with dynamic ordering detected by dc drive, *J. Phys.: Conf. Ser.* **1293**, 012023 (2019).
- [39] A. Zettl and G. Grüner, Phase coherence in the current-carrying charge-density-wave state: Ac-dc coupling experiments in  $\text{NbSe}_3$ , *Phys. Rev. B* **29**, 755 (1984).
- [40] S. N. Coppersmith and P. B. Littlewood, Interference Phenomena and Mode Locking in the Model of Deformable Sliding Charge-Density Waves, *Phys. Rev. Lett.* **57**, 1927 (1986).
- [41] R. E. Thorne, J. R. Tucker, and J. Bardeen, Experiment Versus the Classical Model of Deformable Charge-Density Waves: Interference Phenomena and Mode Locking, *Phys. Rev. Lett.* **58**, 828 (1987).
- [42] M. J. Higgins, A. A. Middleton, and S. Bhattacharya, Scaling Near Mode Locking in a Charge Density Wave Conductor, *Phys. Rev. Lett.* **70**, 3784 (1993).
- [43] S. P. Benz, M. S. Rzchowski, M. Tinkham, and C. J. Lobb, Fractional Giant Shapiro Steps and Spatially Correlated Phase Motion in 2D Josephson Arrays, *Phys. Rev. Lett.* **64**, 693 (1990).
- [44] K. H. Lee, D. Stroud, and J. S. Chung, Calculation of Giant Fractional Shapiro Steps in Josephson-Junction Arrays, *Phys. Rev. Lett.* **64**, 962 (1990).
- [45] M. P. N. Juniper, A. V. Straube, R. Besseling, D. G. A. L. Aarts, and R. P. A. Dullens, Microscopic dynamics of synchronization in driven colloids, *Nat. Commun.* **6**, 7187 (2015).
- [46] A. T. Fiory, Quantum Interference Effects of a Moving Vortex Lattice in Al Films, *Phys. Rev. Lett.* **27**, 501 (1971).
- [47] A. Schmid and W. Hauger, On the theory of vortex motion in an inhomogeneous superconducting film, *J. Low Temp. Phys.* **11**, 667 (1973).
- [48] J. M. Harris, N. P. Ong, R. Gagnon, and L. Taillefer, Washboard Frequency of the Moving Vortex Lattice in  $\text{YBa}_2\text{Cu}_3\text{O}_{6.93}$  Detected by Ac-Dc Interference, *Phys. Rev. Lett.* **74**, 3684 (1995).
- [49] L. Van Look, E. Rosseel, M. J. Van Bael, K. Temst, V. V. Moshchalkov, and Y. Bruynseraede, Shapiro steps in a superconducting film with an antidot lattice, *Phys. Rev. B* **60**, R6998 (1999).
- [50] A. B. Kolton, D. Domínguez, and N. Grønbech-Jensen, Mode Locking in ac-Driven Vortex Lattices with Random Pinning, *Phys. Rev. Lett.* **86**, 4112 (2001).
- [51] N. Kokubo, R. Besseling, V. M. Vinokur, and P. H. Kes, Mode Locking of Vortex Matter Driven through Mesoscopic Channels, *Phys. Rev. Lett.* **88**, 247004 (2002).
- [52] N. Kokubo, K. Kadowaki, and K. Takita, Peak Effect and Dynamic Melting of Vortex Matter in  $\text{NbSe}_2$  Crystals, *Phys. Rev. Lett.* **95**, 177005 (2005).
- [53] S. Okuma, J. Inoue, and N. Kokubo, Suppression of broadband noise at mode locking in driven vortex matter, *Phys. Rev. B* **76**, 172503 (2007).

- [54] S. Okuma, H. Imaizumi, and N. Kokubo, Intrinsic quantum melting of a driven vortex lattice in amorphous  $\text{Mo}_x\text{Ge}_{1-x}$  films, *Phys. Rev. B* **80**, 132503 (2009).
- [55] S. Okuma, H. Imaizumi, D. Shimamoto, and N. Kokubo, Quantum melting and lattice orientation of driven vortex matter, *Phys. Rev. B* **83**, 064520 (2011).
- [56] S. Okuma, D. Shimamoto, and N. Kokubo, Velocity-induced reorientation of a fast driven Abrikosov lattice, *Phys. Rev. B* **85**, 064508 (2012).
- [57] A. Ochi, Y. Kawamura, T. Inoue, T. Kaji, D. Mihaly, S. Kaneko, N. Kokubo, and S. Okuma, Dynamic melting of driven Abrikosov lattices in an amorphous  $\text{Mo}_x\text{Ge}_{1-x}$  film in tilted field, *J. Phys. Soc. Jpn.* **85**, 034712 (2016).
- [58] A. Ochi, N. Sohara, S. Kaneko, N. Kokubo, and S. Okuma, Equilibrium and dynamic vortex states near absolute zero in a weak pinning amorphous film, *J. Phys. Soc. Jpn.* **85**, 044701 (2016).
- [59] S. Shapiro, Josephson Currents in Superconducting Tunneling: The Effect of Microwaves and Other Observations, *Phys. Rev. Lett.* **11**, 80 (1963).
- [60] A. B. Kolton, D. Domínguez, and N. Grønbech-Jensen, Mode locking in driven vortex lattices with transverse ac drive and random pinning, *Phys. Rev. B* **65**, 184508 (2002).
- [61] S. Okuma, K. Kashiro, Y. Suzuki, and N. Kokubo, Order-disorder transition of vortex matter in  $a\text{-Mo}_x\text{Ge}_{1-x}$  films probed by noise, *Phys. Rev. B* **77**, 212505 (2008).
- [62] T. Nishio, S. Okayasu, J. Suzuki, N. Kokubo, and K. Kadowaki, Observation of an extended magnetic field penetration in amorphous superconducting MoGe films, *Phys. Rev. B* **77**, 052503 (2008).
- [63] S. Maegochi, K. Ienaga, S. Kaneko, and S. Okuma, Critical behavior near the reversible-irreversible transition in periodically driven vortices under random local shear, *Sci. Rep.* **9**, 16447 (2019).
- [64] S. Maegochi, K. Ienaga, and S. Okuma, Critical behavior of density-driven and shear-driven reversible-irreversible transitions in cyclically sheared vortices, *Sci. Rep.* **11**, 19280 (2021).
- [65] C. J. Olson Reichhardt, E. Groopman, Z. Nussinov, and C. Reichhardt, Jamming in systems with quenched disorder, *Phys. Rev. E* **86**, 061301 (2012).
- [66] H. Péter, A. Libál, C. Reichhardt, and C. J. O. Reichhardt, Crossover from jamming to clogging behaviors in heterogeneous environments, *Sci. Rep.* **8**, 10252 (2018).
- [67] C. Reichhardt and C. J. O. Reichhardt, Controlled Fluidization, Mobility, and Clogging in Obstacle Arrays using Periodic Perturbations, *Phys. Rev. Lett.* **121**, 068001 (2018).
- [68] R. L. Stoop and P. Tierno, Clogging and jamming of colloidal monolayers driven across disordered landscapes, *Commun. Phys.* **1**, 68 (2018).
- [69] S. O. Valenzuela, Order and Mobility of Solid Vortex Matter in Oscillatory Driving Currents, *Phys. Rev. Lett.* **88**, 247003 (2002).